BMC Medical Imaging

RESEARCH

Open Access

Radiomics model building from multiparametric MRI to predict Ki-67 expression in patients with primary central nervous system lymphomas: a multicenter study

Yelong Shen[1,2†], Siyu Wu[1,2†], Yanan Wu[1], Chao Cui[3], Haiou Li[4], Shuang Yang[5], Xuejun Liu[6], Xingzhi Chen[7], Chencui Huang[7] and Ximing Wang[1,2*]

Abstract

Objectives To examine the correlation of apparent diffusion coefficient (ADC), diffusion weighted imaging (DWI), and T1 contrast enhanced (T1-CE) with Ki-67 in primary central nervous system lymphomas (PCNSL). And to assess the diagnostic performance of MRI radiomics-based machine-learning algorithms in differentiating the high proliferation and low proliferation groups of PCNSL.

Methods 83 patients with PCNSL were included in this retrospective study. ADC, DWI and T1-CE sequences were collected and their correlation with Ki-67 was examined using Spearman's correlation analysis. The Kaplan-Meier method and log-rank test were used to compare the survival rates of the high proliferation and low proliferation groups. The radiomics features were extracted respectively, and the features were screened by machine learning algorithm and statistical method. Radiomics models of seven different sequence permutations were constructed. The area under the receiver operating characteristic curve (ROC AUC) was used to evaluate the predictive performance of all models. DeLong test was utilized to compare the differences of models.

Results Relative mean apparent diffusion coefficient (rADCmean) (ρ=-0.354, $p=0.019$), relative mean diffusion weighted imaging (rDWImean) (b = 1000) (ρ = 0.273, $p=0.013$) and relative mean T1 contrast enhancement (rT1-CEmean) (ρ = 0.385, $p=0.001$) was significantly correlated with Ki-67. Interobserver agreements between the two radiologists were almost perfect for all parameters (rADCmean ICC = 0.978, 95%CI 0.966–0.986; rDWImean (b = 1000) ICC = 0.931, 95% CI 0.895–0.955; rT1-CEmean ICC = 0.969, 95% CI 0.953–0.980). The differences in PFS ($p=0.016$) and OS ($p=0.014$) between the low and high proliferation groups were statistically significant. The best prediction model

†Yelong Shen and Siyu Wu contributed equally to this work.

*Correspondence:
Ximing Wang
wxming369@163.com

Full list of author information is available at the end of the article

in our study used a combination of ADC, DWI, and T1-CE achieving the highest AUC of 0.869, while the second ranked model used ADC and DWI, achieving an AUC of 0.828.

Conclusion rDWImean, rADCmean and rT1-CEmean were correlated with Ki-67. The radiomics model based on MRI sequences combined is promising to distinguish low proliferation PCNSL from high proliferation PCNSL.

Keywords Primary central nervous system lymphoma, Ki-67, Multiparametric magnetic resonance imaging, Radiomics

Introduction

Primary central nervous system lymphoma (PCNSL) is a rare malignant non-Hodgkin's lymphoma (NHL) [1]. PCNSL has irreversible consequences of central nervous system symptoms, and untreated PCNSL has an inferior prognosis with an overall survival (OS) of approximately 1.5 months [2]. To this day, combination therapy with high-dose methotrexate (HD-MTX) and whole-brain radiotherapy (WBRT) improved outcomes with a median disease-free survival of 40.3 months. However, this kind of therapy resulted in severe neurological deficits [3]. Therefore, it is necessary to clarify the diagnosis as soon as possible to avoid the side effects caused by the combined treatment. Stereotactic biopsy is regarded as the gold standard to diagnose PCNSL, but due to its surgical sequelae, a non-invasive method for monitoring tumor progression is required.

Ki-67 can evaluate the proliferative activity of malignant tumors, which reflects the neoplasm invasion [4]. In some malignant tumors, there is a correlation between the expression level of Ki-67 and the prognosis of patients, such as non-Hodgkin's lymphoma and follicular lymphoma [5, 6]. In these tumors, higher levels of Ki-67 expressionis associated with a poorer patient-survival rate. For other tumors, previous studies have demonstrated a significant correlation between apparent diffusion coefficient (ADC) parameters and Ki-67 expression, reflecting tumor biology in terms of proliferative activity [7, 8]. According to these researches, if MRI parameters are related to the expression of Ki-67, we can infer that MRI can reflect the proliferative activity of PCNSL.

MRI is a routine and effective imaging method for the diagnosis of PCNSL. Diffusion-weighted imaging (DWI), and T1 contrast-enhanced (T1-CE) images are more advantageous in identifying PCNSL [9, 10]. MRI (DWI and T1-CE) is also recommended for the diagnosis and evaluation of PCNSL in the 2022 Chinese expert consensus [11]. In malignant tumors, tumor growth can lead to a reduction in the volume of the extracellular space outside the blood vessels which can affect water diffusion [12]. Thus, it leads to a significantly high signal of PCNSL on DWI. In addition, tumor cells destroyed the blood-brain barrier, resulting in significant enhancement on T1-CE MRI [13]. Therefore, we choose ADC, DWI, and T1-CE image to find their correlation with Ki-67. However, the MRI diagnosis of PCNSL still relies on the personal experience and subjective judgment of the radiologist. As a result, the objectivity and stability of the diagnostic process are limited to some extent.

Radiomics is an emerging field in quantitative imaging that uses advanced imaging features to objectively and quantitatively describe tumor phenotypes [14–16]. Radiomics can provide a basis for treatment decisions by modeling and analyzing radiomics features in medical images, which can also be used to predict the prognosis of diseases [17–19].

The purpose of this study was to explore the correlation of ADC, DWI and T1-CE MRI parameters with Ki-67 in PCNSL. The low and high proliferation groups of PCNSL were defined by Ki-67 and used to evaluate the diagnostic performance of the MRI radiomics-based machine learning algorithm in differentiating the low and high proliferation groups of PCNSL. Then we try to modulate the radiomics model based on ADC, DWI, T1-CE and their combinations to find the best sequence to differentiate the low and high proliferation groups of PCNSL.

Materials and methods

Patients

This study included 83 PCNSL patients with complete ADC, DWI and T1-CE MRI image data, clinic-pathological features, and follow-up information. The imaging data of 145 patients were retrospectively collected from March 2019 to September 2021 at the picture archiving and communication systems (PACS) of Shandong Provincial Hospital Affiliated to Shandong First Medical University, Qilu Hospital of Shandong University, Shandong Cancer Hospital and Institute, the Affiliated Hospital of Qingdao University and Shandong Provincial Qianfoshan Hospital. MRI images included in the study were obtained from each center prior to biopsy, surgery and any treatment. Inclusion criteria included: (1) PCNSL was confirmed by stereotactic biopsy with Ki-67 by immunohistochemical examination; (2) No other lymphoma; (3) Complete MRI examination data with DWI (b = 1000), ADC and T1-CE images; (4) No history of congenital or acquired immune deficiency. Exclusion criteria were as follows: (1) Absence of clinical information and imaging; (2) Poor image quality; (3) Prior to the MRI, the patient had a history of treatment for PCNSL (puncture, surgery, steroid therapy,

radiotherapy and chemotherapy). Survival and treatment outcomes were documented by telephone follow-up. Progression-free survival (PFS) was defined as the time from initial treatment to disease progression, relapse, or death, whereas overall survival (OS) was defined as the time from initial diagnosis to death from any cause. Finally, 83 patients were enrolled in this study and randomly assigned to the training set ($n = 58$) and the test set ($n = 25$) in a ratio of 7:3 (Fig. S1).

MRI examinations

All images were acquired during routine clinical examination using 3.0T MRI scanners and their matching head phased array coils. More details of the scanning parameters are available in the Supplement Materials and Methods section of the Supplementary Material.

Image analysis

All images were analyzed by two experienced radiologists (both with 10 years of neuro-MRI diagnostic experience) without knowledge of the histopathological diagnosis.

Image analysis was performed on a Siemens SIENET Magic View 1000 console prior to stereotaxic biopsy. The lesion in question was identified by a neurosurgeon with a stereotaxic biopsy. DWI (b = 1000) and ADC maps were registered with T1-CE MRI for improved visualization and correlation. The radiologist then viewed the co-registered DWI (b = 1000), ADC maps, and T1-CE images and outlined the entire enhancement as the region of interest (ROI) at the largest cross-section of the tumor and obtained the T1-CE mean signal value of the lesion by Siemens Syngo. via (Munich, Germany). Finally, ADC and DWI mean signal values of the lesion were obtained by copying the measurement of the ROI and pasting it to the same organ position on the corresponding ADC and DWI images. Similarly, T1-CE, ADC and DWI mean signal values of the contralateral thalamus were obtained (Fig. S2). In order to reduce the influence of different scanners or the differences of the background signal, we defined the ratio of the lesion ROI measurement to the contralateral thalamus measurement as the relative mean signal value of the lesion [20, 21]. The relative mean Apparent Diffusion Coefficients (rADCmean), relative mean Diffusion Weighted Imaging (b = 1000) (rDWImean) and relative mean T1 contrast enhanced (rT1-CEmean) of the ROI of each lesion were independently analyzed by two readers. ROI signal values were measured and averaged by two radiologists. The ROI signal values measured by two radiologists were used for inter-observer intraclass correlation coefficient (ICC) analysis, and the average value was used for correlation analysis between MRI parameters and tumor Ki-67.

Histopathological examination and immunohistochemical assay

Neurosurgeons obtained pathological specimens by stereotaxic biopsy. The mean interval between specimen acquisition and MRI examination was 20 days. Analysis and diagnosis by pathologists. Immunohistochemical analysis was performed using antibody against Ki-67 (1:200, Dako). To identify Ki-67-positive tumor cells, we observed and counted at least 1,000 tumor cells in more than five high-power fields, with a relatively uniform distribution of tumor cells. From previous studies [22, 23], Ki-67 ≥ 90% was correlated with OS and PFS in PCNSL. Therefore, Ki-67 was defined as the percentage of total tumor cells with nuclear staining (Ki-67 positive). Meanwhile, we defined Ki-67 < 90% as the PCNSL low proliferation group, and Ki-67 ≥ 90% as the PCNSL high proliferation group.

Image preprocessing

To avoid data heterogeneity bias, resampling and normalization were conducted for DWI, ADC and T1-CE images before radiomics feature extraction. Moreover, nine imaging transformation methods were conducted including wavelet, Laplacian of Gaussian (LoG), Local Binary Pattern (LBP) 2D, LBP 3D, square, square root, logarithm, exponential and gradient filtering.

Feature extraction and selection

In order to evaluate the stability of the extracted radiomics features, we performed inter-observer and intra-observer repeatability analyses. A total of 15 cases were randomly selected to establish two identical DWI image labeling tasks. Observer 1 and Observer 2 (both with 10 years of neuro-MRI diagnostic experience) independently segmented the entire tumor region on consecutive cross-sectional images to obtain the volume of interest (VOI), respectively. The obtained radiomics features were used for ICC analysis between observers. Observer 1 re-segmented the above 15 cases at an interval of one month, and the radiomics features obtained from the first and second segmentation were used for intra-observer ICC analysis; finally, the observer 1 completed the segmentation of all the remaining cases. Then, radiomics features were extracted from the VOI of the three sequences respectively via the Deepwise Multimodal Research Platform (https://keyan.deepwise.com, V2.0) (Beijing Deepwise & League of PHD Technology Co., Ltd., Beijing, China).

The existence of unstable radiomics features and highly correlated radiomics features may influence the model performance, so feature selection is a key step in the model establishment process. First, the unstable radiomics features were removed from the intra-observer and inter-observer ICC analysis results in the feature

extraction step. The radiomics features with high stability between and within observers (ICC ≥ 0.8) were selected for further feature screening. Then, a feature correlation analysis, with a threshold of 0.7, was used to calculate the linear correlation coefficients. One of the features needed to be removed to alleviate the redundancy, when the linear correlation coefficient between any two features was greater than that of the threshold. F test was conducted to screen features further.

Model construction and evaluation

Support vector machine (SVM) is a binary classification model, its learning strategy is to maximize the interval, which can be formalized as a problem of solving convex quadratic programming. Previous studies suggest that SVM is effective in high dimensional feature space, and its sparse feature can suppress data noise [24]. Therefore, the SVM was used for this study.

The data set of 83 samples was randomly split by a ratio of 7:3. 70% of them were used as training set to train the model and 30% of them were used as testing set to validate the model performance. Seven radiomics models were established based on features selected from single-sequence images (DWI, T1-CE, ADC) and multi-sequences images (ADC + DWI, ADC + T1-CE, DWI + T1-CE, ADC + DWI + T1-CE) with SVM algorithm, respectively.

Independent predictors associated with Ki-67 levels were selected using univariate and multivariate logistic regression. Then, a clinical-radiomics model was developed by combining the best radiomics model and the independent predictors associated with Ki-67 levels.

AUC, sensitivity, specificity and accuracy were calculated to evaluate the performance of models. ROC curve was also drawn to assess the distinguishing ability of models. A decision curve was applied to analyze the clinical efficacy of the best machine learning model. The calculation method of net benefit is $\text{Net benefit} = \frac{\text{True Positives}}{\text{n}} - \frac{\text{False Positives}}{\text{n}}\left(\frac{\text{pt}}{1-\text{pt}}\right)$ (**n**: total number of cases; **pt**: threshold probability, where the expected benefit of treatment equals the expected benefit of avoiding treatment) [25]. Moreover, the DeLong test was performed to calculate the statistical differences of models. Figure 1 describes the workflow from image analysis to radiomics model performance evaluation.

Statistical analysis

Variations in clinical factors between the high proliferation and low proliferation groups were evaluated by Chi-squared ($\chi 2$) tests or Mann-Whitney U tests. Survival was assessed by the Kaplan-Meier method in the low proliferation and high proliferation groups and the log-rank test was used for comparison. The relationship of rADCmean, rDWImean, and rT1-CEmean of extracellular matrix in each lesion with Ki-67 was assessed using Spearman's correlation analysis. Univariate logistic regression was applied to select variables with $p < 0.05$, and multivariate logistic regression was performed on these variables to screen for independent predictors of association with Ki-67. DeLong test was used to

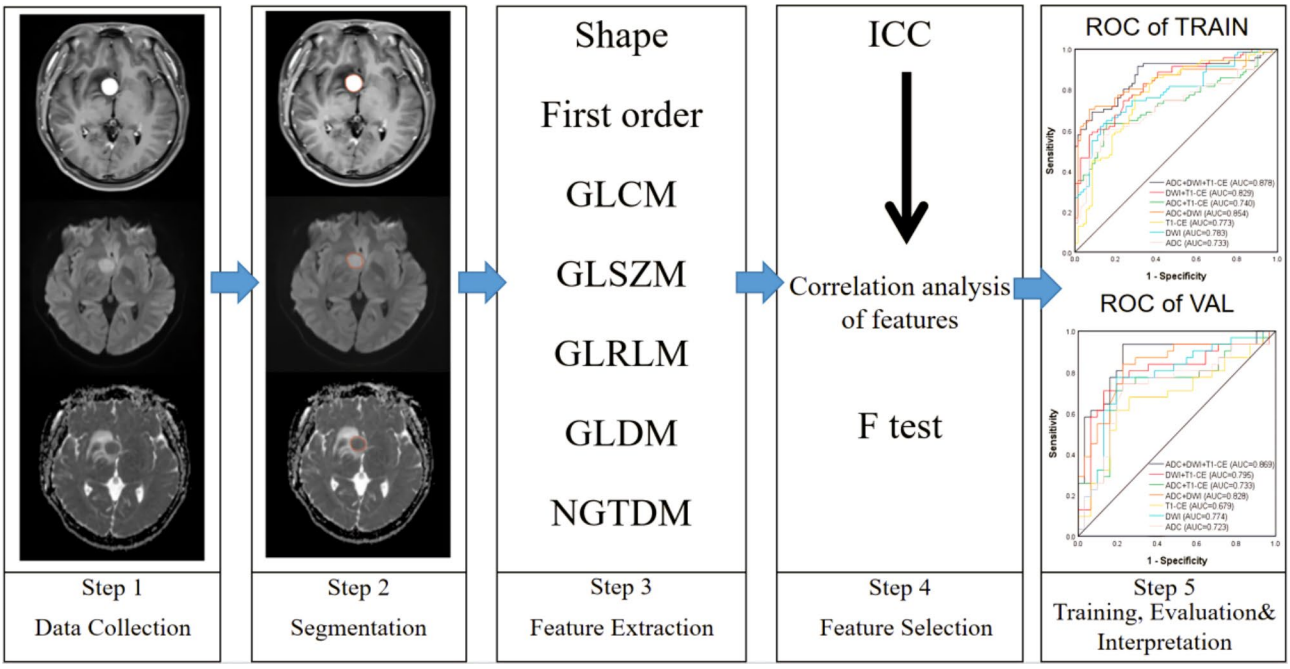

Fig. 1 Overview of the current study workflow. ICC, intraclass correlation coefficient; ROC, receiver operating characteristic

Table 1 Baseline characteristics of participants in Low Proliferation Group and High Proliferation Group

Variable	Low proliferation group (*n* = 54)	High proliferation group (*n* = 29)	*p*
Age (y)*	62 (55.3–67)	60 (52–66)	0.476
Sex (n, %)	29 (53.7)	15 (51.7)	0.863
Immunophenotype (n, %)			0.207
GCB	15 (27.8)	12 (41.3)	
Non-GCB	39 (72.2)	17 (58.6)	
PFS (m)*	32.9 (27.4–40)	31 (25.5–35.5)	**0.016**
OS (m)*	39 (33–43)	32.1 (28–39)	**0.014**

* Data are medians, with IQRs in parentheses

Bold value indicates $p < 0.05$

PFS, progression-free survival; OS, overall survival; GCB, germinal center B cell-like

Table 2 Spearman Correlation Analysis of the relationship between Ki67 and MRI parameters (DWI, ADC and T1-CE)

Parameters	Spearman's ρ	*p* value
rDWImean	0.273	**0.013**
rADCmean	-0.354	**0.019**
rT1-CEmean	0.385	**0.001**

calculate statistical differences of different models via Medcalc (version 11.4.2.0, https://www.medcalc.org). Inter-observer agreement was assessed using the ICC. Statistical analysis and graphing were performed by the Deepwise Multimodal Research Platform and SPSS 25.0. *p* values less than 0.05 were considered to indicate statistical significance.

Results

Correlation between Ki-67 and MRI parameters

Among the 83 lesions, 54 lesions (25 women, 29 men; 28–80 years, mean age 60 years) and 29 lesions (14 women,15 men; 5–73 years, mean age 58 years) were in the low proliferation group and the high proliferation group, respectively. The histological type of all PCNSL was primary diffuse large B-cell CNS lymphoma. The clinical characteristics of the two groups are shown in Table 1. By the end of follow-up, 30 (36.1%) of the 83 patients experienced disease progression or recurrence, and 52 (63.9%) died. When comparing clinical factors, no statistically significant differences in age and gender were observed between the two groups, however, statistically significant differences in PFS ($p = 0.016$) and OS ($p = 0.014$) were observed. The Kaplan-Meier curve indicates that patients in the high proliferation group showed lower PFS and OS (Fig. 2). As shown in Table 2, rADCmean (ρ = -0.354, $p = 0.019$), rDWImean (b = 1000) (ρ = 0.273, $p = 0.013$) and rT1-CEmean (ρ = 0.385, $p = 0.001$) and Ki-67 significant correlation. Figure 3 are representative examples of low and high proliferation groups and their immunohistochemical staining images. As shown in Fig. 4, the inter-observer agreement for all parameters is good.

Feature selection

A total of 1906, 1906 and 1743 radiomics features were extracted from each patient 's ADC, DWI and T1-CE images, respectively. After inter-observer and intra-observer ICC analysis, ADC, DWI and T1-CE retained 1197, 1406 and 1468 features, respectively. Finally, after feature reduction, 11 features of ADC images, 15 features of DWI images and 9 features of T1-CE features were retained. ADC model, DWI model and T1-CE model were established by the SVM algorithm.

Moreover, univariate logistic regression showed that age (≤ 60 vs. >60 years), sex, and immunophenotype (germinal center B cell-like (GCB) vs. non-GCB) were not predictors of Ki-67 LI (Ki-67 < 90 vs. ≥ 90) (Table S1).

Models performance

Based on features from individual MRI sequence, the model achieved an AUC from 0.733 to 0.783 on training set and from 0.679 to 0.774 on testing set. Based on features from a combination of sequences, the model

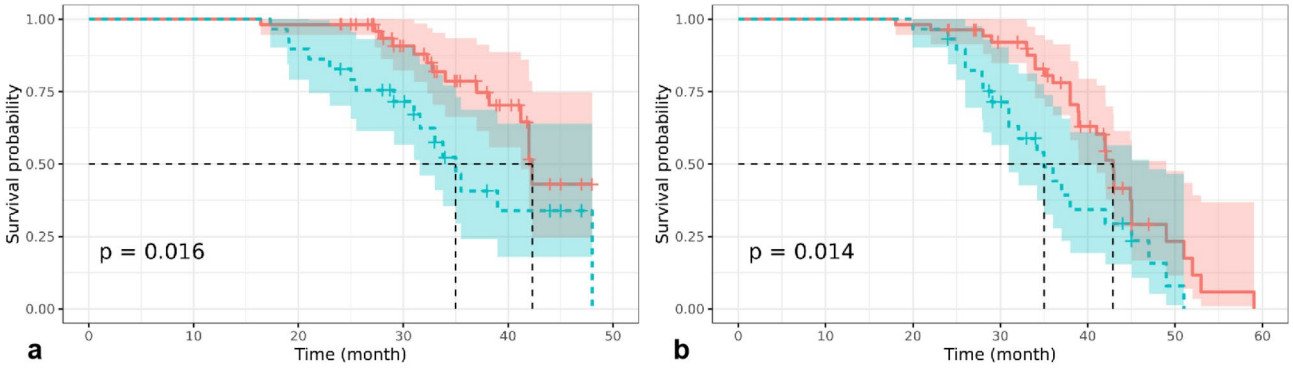

Fig. 2 Kaplan-Meier assessment of the difference in progression-free survival (**a**) and the difference in overall survival (**b**) between the low proliferation group (red line) and the high proliferation group (green line)

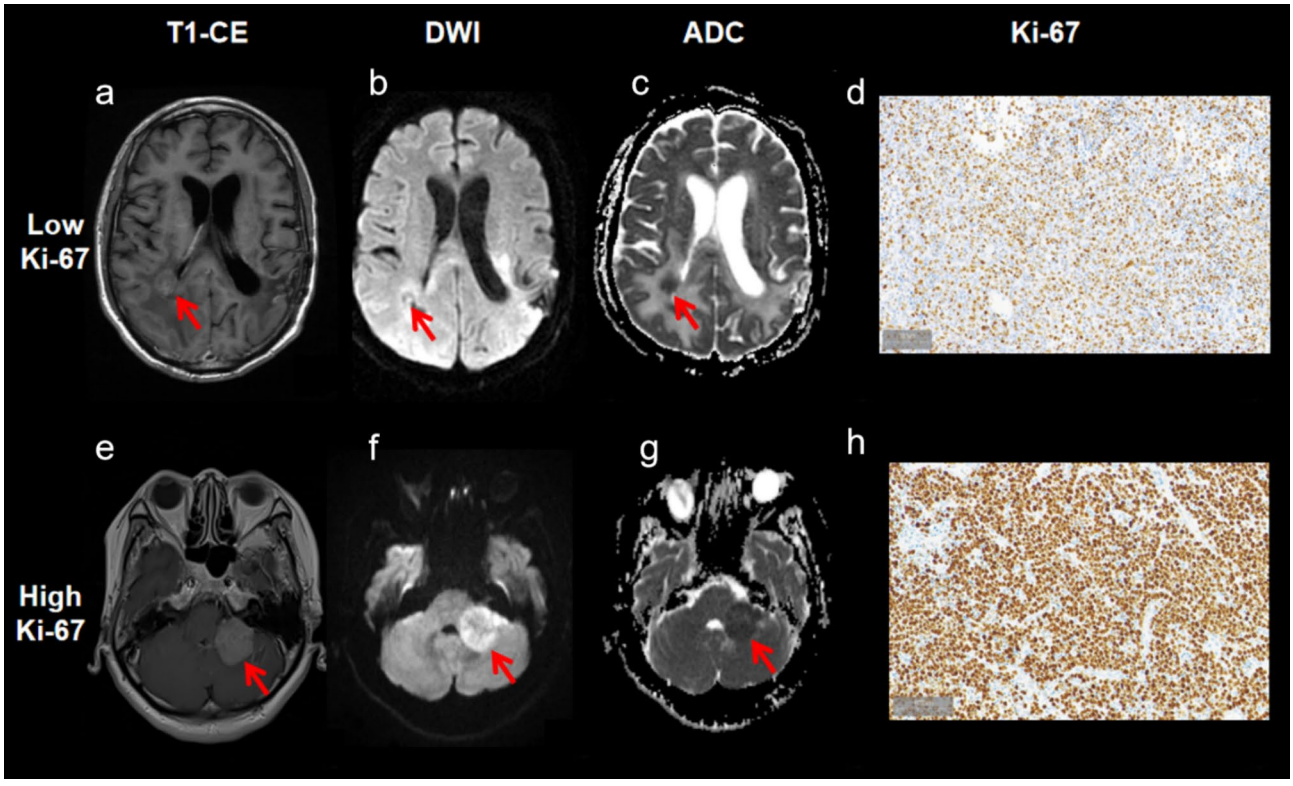

Fig. 3 Representative examples of low proliferation group (**a-c**) and high proliferation group (**e-g**), and their immunohistochemical staining images (**d** and **h**). **a** Brain axial T1-CE showed right occipital lobe mass (arrow) significantly enhanced lesions around the patchy low intensity edema. The rT1-CEmean was 1.57. **b** Brain DWI showed significantly low signal in the necrotic area of the lesion (arrow) and significantly high signal in the solid part. The rDWImean was 1.29. **c** Intracranial ADC showed low signal in the solid part of the lesion (arrow) and obvious high signal in the surrounding edema. The rADCmean is 1.82. **d** Representative microscopic images at×200 magnification showed partial Ki-67-stained tumor cells, indicating low proliferation; Ki-67 labeling index was 50. **e** Brain axial T1-CE showed left cerebellar mass (arrow) significantly enhanced, no obvious edema around the lesion. The rT1-CEmean was 2.15. **f** DWI of brain showed obvious low signal in the necrotic area of the lesion (arrow) and obvious high signal in the solid part. The rDWImean was 1.69. **g** Intracranial ADC showed low signal in the solid portion of the lesion (arrow), and high signal in the surrounding edema. The rADCmean is 1.59. **h** Representative microscopic images at×200 magnification showed a large number of Ki-67-stained tumor cells, indicating high proliferation; Ki-67 labeling index was 90

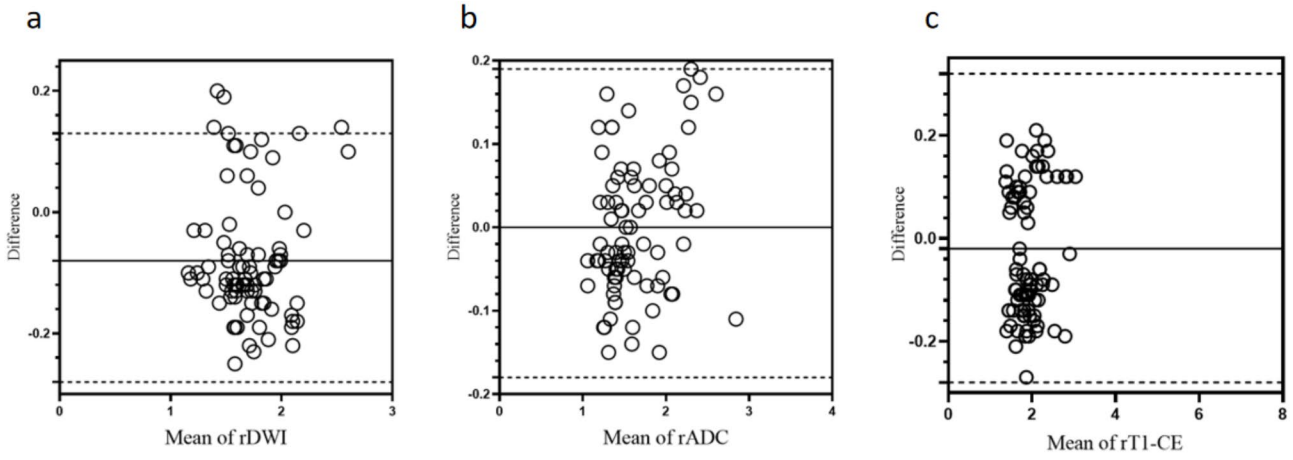

Fig. 4 Bland-Altman plots of rDWI (**a**), rADC (**b**) and rT1-CE (**c**) demonstrating agreement between the values measured by the two radiologists. Differences (y-axis) between measurements obtained by two radiologists are plotted against the mean values (x-axis) of the measurements obtained by them. Solid line, top and bottom dashed lines indicate the mean difference, and the upper and lower margins of 95% limits of agreement, respectively

Table 3 AUC, Accuracy, specificity, and sensitivity on training and testing sets of different models

	Metrics	ADC + DWI + T1-CE	ADC + DWI	DWI + T1-CE	ADC + T1-CE	ADC	T1-CE	DWI
Training set	AUC	0.878	0.854	0.829	0.740	0.733	0.773	0.783
	Accuracy	0.803	0.782	0.732	0.739	0.718	0.725	0.725
	Sensitivity	0.686	0.586	0.676	0.643	0.614	0.789	0.676
	Specificity	0.917	0.972	0.789	0.833	0.819	0.662	0.775
Testing set	AUC	0.869	0.828	0.795	0.733	0.723	0.679	0.774
	Accuracy	0.742	0.710	0.758	0.742	0.710	0.613	0.726
	Sensitivity	0.645	0.516	0.645	0.677	0.613	0.677	0.613
	Specificity	0.839	0.903	0.871	0.807	0.807	0.548	0.839

AUC area under the curve

Table 4 DeLong test results for the best performing Radiomics Model and other Radiomics models

	P value of the training set	*P* value of the testing set
all VS. T1-CE	**0.025**	**0.002**
all VS.ADC	**0.001**	**0.007**
all VS.DWI	**0.035**	0.188
all VS. T1-CE + ADC	**0.001**	**0.006**
all VS. T1-CE + DWI	0.204	0.143
all VS. ADC + DWI	0.387	0.055

Bold value indicates $p < 0.05$

achieved an AUC from 0.740 to 0.854 on training set and from 0.733 to 0.828 on testing set. Based on features combined all different sequences, the model had the best performance with an AUC of 0.878 on training set and an AUC of 0.869 on testing set. The results are shown in Table 3. Moreover, there is a significant difference between the ADC + DWI + T1-CE model and the ADC model ($p = 0.001$), DWI model ($p = 0.035$) and T1-CE model ($p = 0.025$) on the training set, respectively. And there was a significant difference between the ADC + DWI + T1-CE model and the ADC model ($p = 0.007$) and T1-CE model ($p = 0.002$) on testing set, respectively, as shown in Table 4. Detailed information on the DeLong test of the other models is provided in Table S2.

Figure 5 showed that the model of all sequences combined had the highest AUC on both training and testing sets and the best prediction performance.

To analyze the clinical value of the best ADC + DWI + T1-CE model, we plotted a decision curve shown in Fig. 6. We found that the net clinical benefit obtained by the model was greater than the net clinical

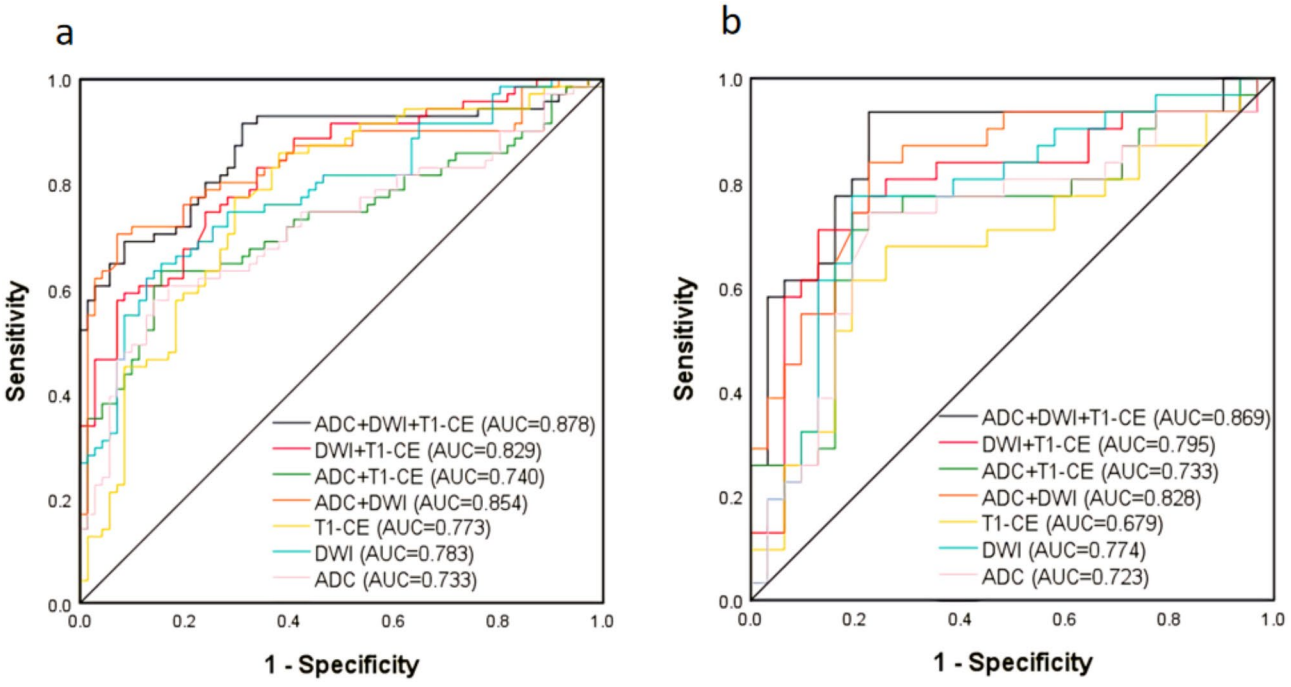

Fig. 5 Receiver operating characteristic (ROC) curve of all the models in training set (**a**) and validation set (**b**)

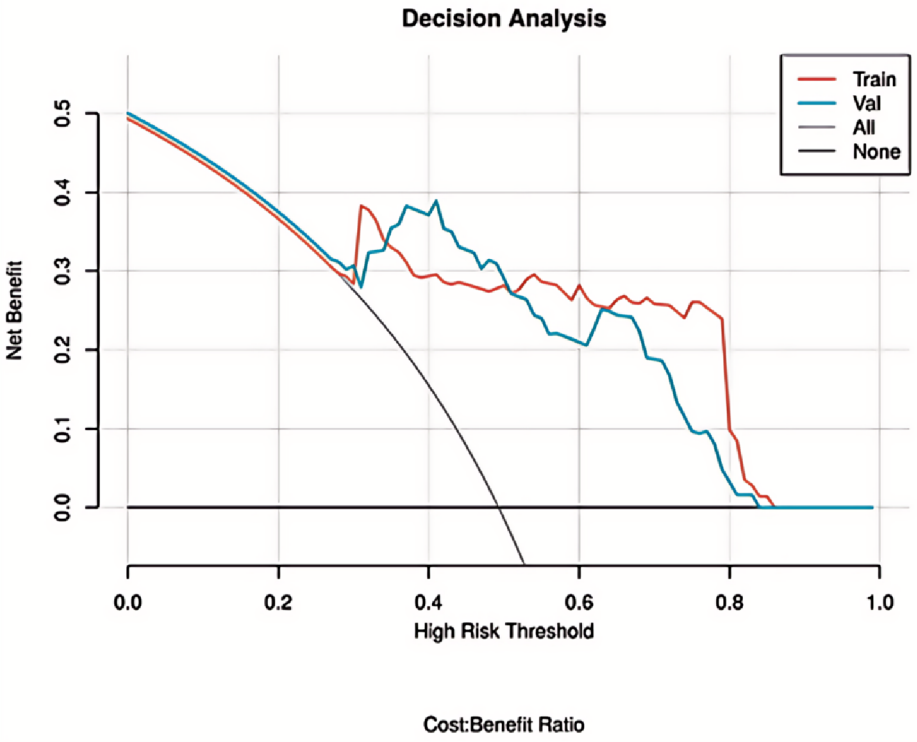

Fig. 6 Decision curve of the model built by all sequences combined

benefit of classifying all patients and not classifying all patients.

Discussion

The incidence of PCNSL has been steadily rising over the last 30 years [26]. Due to the lack of specific clinical manifestations, there is a certain misdiagnosis rate in imaging diagnosis [27, 28]. The treatment method of PCNSL is different from that of conventional tumors. The treatment of PCNSL is mainly combined with HD-MTX chemotherapy and WBRT (45 Gy) [11]. Hence, early diagnosis is crucial to avoid unnecessary surgical resection [3, 29]. Furthermore, early diagnosis and follow-up examination after therapy play a crucial role in the prognosis of PCNSL [30]. Because patients in the high proliferation group had significantly lower PFS ($p = 0.016$) and OS ($p = 0.014$) than those in the low proliferation group, accurate prediction of tumor proliferation levels prior to treatment can help clinicians risk stratify and develop appropriate treatment regimens and follow-up strategies [31, 32]. The radiomics model we developed was able to grade tumors by analyzing MRI images (ADC, DWI and T1-CE).

Previous studies have shown that Ki-67 could indicate tumor aggressiveness and it is an important predictor for disease prognosis [33–35]. Ki-67 is an independent prognostic factor in determining post-metastatic overall survival (PMOS) in certain malignancies [36]. Furthermore, in breast cancer patients, the Ki-67 expression level was an independent predictor of significant disease response to neoadjuvant chemotherapy [37]. It is closely related to the increase of cell number and volume, and this will restrict the diffusion of water molecules which increase the signal of DWI. At the same time, high levels of Ki-67 also represent a strong invasive ability of the tumor, that is, the ability to infiltrate and destroy blood vessels. PCNSL lesions usually have cuffing infiltration around blood vessels which destroys vascular endothelial cells. In this case, the contrast agent seeps from the damaged blood-brain barrier around the tumor. As a result, hypo-vascular PCNSL is often markedly homogeneously enhanced on T1-CE images. Moreover, the higher the level of Ki-67, the more active the proliferation of tumor cells. The greater the damage to the blood-brain barrier, the more obvious the tumor enhanced. Therefore, to find whether ADC, DWI and T1-CE parameters are related to Ki-67 levels in primary CNS lymphoma is important for interpreting the biological significance of medical images. The relative mean signal value (rDWImean, rADCmean and rT1-CEmean) is stable throughout the various MRI vendors and thus could be regarded as reliable. In this study, we found that rDWImean, rADCmean and rT1-CEmean were significantly associated with Ki-67. Consequently, the rDWImean, rADCmean and rT1-CEmean utilized in this study can conveniently filter

PCNSL patients with high levels of Ki-67 in a rapid pace of clinical work [38, 39].

ADC can detect the diffusion of water molecules in lesions to reflect the microstructure of lesions. A significant negative correlation between Ki-67 and ADC parameters was observed in breast cancer [40] and liver cancer [41]. In the study of Schob et al. [42], Ki-67 also showed a significant negative correlation with ADC fractions in PCNSL. This is consistent with our results. The results of this study showed that rT1-CEmean was significantly correlated with Ki-67, and there was a significant difference between the high proliferation group and the low proliferation group. Notably, Schmitz et al. found that conventional imaging features based on T1-CE and MRI radiomics features could differentiate between low-proliferative and high-proliferative soft tissue sarcomas [43]. This suggests that in certain malignant tumors, T1-CE properties could correlate with Ki-67, potentially aiding in the initial screening of tumors with high proliferative activity. Such a relationship may allow for better early identification of highly proliferative malignancies, which are typically associated with poorer prognosis.

More and more studies have focused on radiomics for the prediction of disease treatment response [44], prognosis prediction [45], exploring the relationship between radiomics features and biological features [46–48]. Based on the above research results, we developed a radiomics model that can predict the proliferation level of PCNSL. In order to ensure the reliability of the prediction model, this study excluded variable factors by three steps. Firstly, in order to reduce the adverse effects caused by the singular sample data, we standardized and normalized the data. Then radiomics features were extracted from each patient's ADC, DWI, and T1-CE images, respectively. The second step is to exclude the differences between radiologists in describing ROI and select omics features with high stability (ICC ≥ 0.8) for the next feature screening. The last step is to adjust the threshold of feature correlation analysis and use the F test for feature screening.

Age of PCNSL patients was strongly associated with prognosis [49], however, age, sex, and immunophenotype were not found to be predictors of Ki-67 LI in our study, similar to past studies [50]. Therefore, this study developed MRI-based radiomics model that did not include clinical factors to establish a clinical-radiomics model. This may be an advantage of this study because patients in the high proliferation group can be detected using only MRI images without considering clinical factors, which makes it more convenient in the application process.

ROC curve showed that the model constructed by all sequences combined, sequence combination (DWI + T1-CE) and radiomics features in T1-CE images had good diagnostic performance. The AUC of all sequence combination validation sets was 0.869 (95% CI 0.772–0.966), which had the best diagnostic performance. The reason is that radiomics features based on multiple sequences can independently and perfectly describe tumor information and are significantly correlated with Ki-67.

Radiomics can extract high throughput quantitative image features to characterize lesion features [51]. These features include geometry, signal intensity histogram, and image texture features to reflect the level of tumor proliferation and may explain the difference between the high and low proliferation groups of PCNSL [52]. Most of the features cannot be visually obtained by the naked eye, so the number is far more than the imaging features observed by the naked eye of radiologists. Therefore, the model's description of the tumor may be more perfect, which has been confirmed in the study of Xia et al. [53]. Previous studies have constructed radiomics models with good diagnostic performance for the diagnosis of typical or atypical PCNSL and the differential diagnosis of PCNSL and glioma, helping clinicians to diagnose patients who cannot undergo stereotactic biopsy [54, 55]. The radiomics model constructed in this study may help to predict the tumor proliferation level of patients with stereotactic biopsy contraindications and provide more reliable decision support for tumor treatment and reexamine after treatment. This model could be beneficial to avoid the optimal treatment time window missing for patients with biopsy contraindications and to enable personalized medicine.

The decision analysis curve has unique advantages in analyzing the clinical value of the model. We found that in the test set, the model achieved a net clinical benefit after grouping patients for Ki-67 compared to no grouping patients. Therefore, radiomic models can predict the disease prognosis and provide clinical treatment decision support.

Our study has some limitations. First of all, due to the low incidence of PCNSL, this study was conducted retrospectively, which may limit the generalizability and representativeness of the results. Therefore, future research should further validate the reliability of our findings in prospective cohorts. In addition, the ability of the scientific research platform used in this study to extract features is limited. While current feature extraction method provides some insights, the introduction of more advanced techniques and algorithms will help improve the granularity and adaptability of feature extraction. In future work, we expect to be able to optimize the process using more powerful platforms in order to obtain more comprehensive data support. Furthermore, the manual approach of outlining the entire enhancement may introduce inter- and intra-observer variability. Future studies should focus on the development of deep learning models for automated lesion recognition to mitigate

this variability. Finally, due to the lack of specific clinical manifestations of PCNSL, this study did not construct a nomogram in combination with clinical factors, and past studies have shown that nomograms perform significantly better than routinely used clinical tumor staging, tumor size and clinical models [56]. Therefore, in future work, more clinical factors of PCNSL need to be extracted and combined with radiomics features to show nomogram.

Conclusion

This study found that rDWImean, rADCmean and rT1-CEmean were associated with Ki-67, demonstrating that the relative mean signal value of MRI may provide some insight into assessing the level of PCNSL proliferation. Furthermore, this study demonstrates that MRI radiomics-based machine learning algorithms have good diagnostic performance in distinguishing high and low proliferation groups of PCNSL, which deserves further exploration and validation.

Abbreviations

ADC	Apparent diffusion coefficient
AUC	Area under the curve
DWI	Diffusion weighted imaging
GCB	Germinal center B cell-like
HD-MTX	High-dose methotrexate
ICC	Interclass correlation coefficient
LI	Labeling index
NHL	Non-Hodgkin's lymphoma
OS	Overall survival
PACS	Picture archiving and communication systems
PCNSL	Primary central nervous system lymphoma
PFS	Progression-free survival
ROC	Receiver operating characteristic
rADCmean	Relative mean apparent diffusion coefficient
rDWImean	Relative mean diffusion weighted imaging
rT1-CEmean	Relative mean T1 contrast enhancement
SVM	Support vector machine
T1-CE	T1 contrast enhanced
TE	Echo time
TR	Repetition time
VOI	Volume of interest
WBRT	Whole-brain radiotherapy

Supplementary Information

The online version contains supplementary material available at https://doi.org/10.1186/s12880-025-01585-5 .

Supplementary Material 1

Acknowledgements

The authors would like to thank all the participants.

Author contributions

Yelong Shen: Data curation, Formal analysis, Methodology, Project. Siyu Wu: Formal analysis, Methodology, Visualization, Writing– original draft, Writing– review & editing. Yanan Wu: Data curation. Chao Cui: Data curation. Haiou Li: Data curation. Shuang Yang: Data curation. Xuejun Liu: Data curation. Xingzhi Chen: Project. Chencui Huang: Project. Ximing Wang: Conceptualization, Data curation, Project administration, Supervision, Writing– review & editing. All authors reviewed the manuscript.

Funding

The present study was supported by the National Natural Science Foundation of China (Grant Nos. 82271993, 82471978).

Data availability

The data that support the findings of this study are available from the corresponding author, upon reasonable request.

Declarations

Ethics approval and consent to participate

This retrospective study was approved by the Ethics Committee of the Shandong Provincial Hospital and written informed consent for the participants over 16 years of age was discarded because of the retrospective nature of this study. For participants less than 16 years of age, written informed consent has been obtained from their parents/guardians after a brief description of the purpose and objectives of the study has been given to them. We confirmed that the study was carried out in accordance with relevant guidelines and regulations of Helsinki Declaration.

Consent for publication

Not applicable.

Competing interests

The authors declare no competing interests.

Clinical trial number

Not applicable.

Author details

[1]Department of Radiology, Shandong Provincial Hospital, No. 324, Jingwu Road, Jinan 250021, Shandong, China
[2]Department of Radiology, Shandong University, No. 44, West Wenhua Road, Jinan 250021, Shandong, China
[3]Qilu Hospital of Shandong University Dezhou Hospital, Dezhou 253000, Shandong, China
[4]Cheeloo College of Medicine, Qilu Hospital, Shandong University, Jinan 250021, Shandong, China
[5]Department of Radiology, The First Affiliated Hospital of Shandong First Medical University& Shandong Provincial Qianfoshan Hospital, Jinan 250021, Shandong, China
[6]Department of Radiology, the Affiliated Hospital of Qingdao University, Qingdao 266000, Shandong, China
[7]Department of Research Collaboration, R&D center, Beijing Deepwise & League of PHD Technology Co., Ltd, 100080 Beijing, China

Received: 18 December 2023 / Accepted: 10 February 2025
Published online: 17 February 2025

References

1. Farrall AL, Smith JR. Changing incidence and survival of primary Central Nervous System Lymphoma in Australia: a 33-Year National Population-based study. Cancers (Basel) 2021, 13(3).https://www.ncbi.nlm.nih.gov/pubmed/33499081
2. Han CH, Batchelor TT. Diagnosis and management of primary central nervous system lymphoma. Cancer. 2017;123(22):4314–24. https://www.ncbi.nlm.nih.gov/pubmed/28950405.
3. Bairey O, Siegal T. The possible role of maintenance treatment for primary central nervous system lymphoma. Blood Rev. 2018;32(5):378–86. https://www.ncbi.nlm.nih.gov/pubmed/29551465.
4. Bi S, Li J, Wang T, Man F, Zhang P, Hou F, Wang H, Hao D. Multi-parametric MRI-based radiomics signature for preoperative prediction of Ki-67 proliferation status in sinonasal malignancies: a two-centre study. Eur Radiol. 2022;32(10):6933–42. https://www.ncbi.nlm.nih.gov/pubmed/35687135.
5. Maeshima AM, Taniguchi H, Hori Y, Ida H, Hosoba R, Makita S, Fukuhara S, Munakata W, Suzuki T, Maruyama D, et al. Diagnostic utility and prognostic significance of the Ki-67 labeling index in diffuse large B-cell lymphoma transformed from follicular lymphoma: a study of 76 patients. Pathol Int. 2021;71(10):674–81. https://www.ncbi.nlm.nih.gov/pubmed/34339560.

6. Vogt N, Klapper W. Variability in morphology and cell proliferation in sequential biopsies of mantle cell lymphoma at diagnosis and relapse: clinical correlation and insights into disease progression. Histopathology. 2013;62(2):334–42. https://www.ncbi.nlm.nih.gov/pubmed/23240716.
7. Andre F, Ismaila N, Allison KH, Barlow WE, Collyar DE, Damodaran S, Henry NL, Jhaveri K, Kalinsky K, Kuderer NM, et al. Biomarkers for adjuvant endocrine and chemotherapy in early-stage breast Cancer: ASCO Guideline Update. J Clin Oncol. 2022;40(16):1816–37. https://www.ncbi.nlm.nih.gov/pubmed/35439025.
8. Fu F, Sun X, Li Y, Liu Y, Shan Y, Ji N, Wang X, Lu J, Sun S. Dynamic contrast-enhanced magnetic resonance imaging biomarkers predict chemotherapeutic responses and survival in primary central-nervous-system lymphoma. Eur Radiol. 2021;31(4):1863–71. https://www.ncbi.nlm.nih.gov/pubmed/32997181.
9. Kuker W, Nagele T, Korfel A, Heckl S, Thiel E, Bamberg M, Weller M, Herrlinger U. Primary central nervous system lymphomas (PCNSL): MRI features at presentation in 100 patients. J Neurooncol. 2005;72(2):169–77. https://www.ncbi.nlm.nih.gov/pubmed/15925998.
10. Wieduwilt MJ, Valles F, Issa S, Behler CM, Hwang J, McDermott M, Treseler P, O'Brien J, Shuman MA, Cha S, et al. Immunochemotherapy with intensive consolidation for primary CNS lymphoma: a pilot study and prognostic assessment by diffusion-weighted MRI. Clin Cancer Res. 2012;18(4):1146–55. https://www.ncbi.nlm.nih.gov/pubmed/22228634.
11. Chen T, Liu Y, Wang Y, Chang Q, Wu J, Wang Z, Geng D, Yu JT, Li Y, Li XQ, et al. Evidence-based expert consensus on the management of primary central nervous system lymphoma in China. J Hematol Oncol. 2022;15(1):136. https://www.ncbi.nlm.nih.gov/pubmed/36176002.
12. Barajas RF, Politi LS, Anzalone N, Schoder H, Fox CP, Boxerman JL, Kaufmann TJ, Quarles CC, Ellingson BM, Auer D, et al. Consensus recommendations for MRI and PET imaging of primary central nervous system lymphoma: guideline statement from the International Primary CNS Lymphoma Collaborative Group (IPCG). Neuro Oncol. 2021;23(7):1056–71. https://www.ncbi.nlm.nih.gov/pubmed/33560416.
13. Zhang HW, Lyu GW, He WJ, Lei Y, Lin F, Feng YN, Wang MZ. Differential diagnosis of central lymphoma and high-grade glioma: dynamic contrast-enhanced histogram. Acta Radiol. 2020;61(9):1221–7. https://www.ncbi.nlm.nih.gov/pubmed/31902220.
14. Lohmann P, Franceschi E, Vollmuth P, Dhermain F, Weller M, Preusser M, Smits M, Galldiks N. Radiomics in neuro-oncological clinical trials. Lancet Digit Health. 2022;4(11):e841–9. https://www.ncbi.nlm.nih.gov/pubmed/36182633.
15. Zhang L, Sun K, Shi L, Qiu J, Wang X, Wang S. Ultrasound Image-based deep features and Radiomics for the discrimination of small Fat-Poor Angiomyolipoma and Small Renal Cell Carcinoma. Ultrasound Med Biol. 2023;49(2):560–8. https://www.ncbi.nlm.nih.gov/pubmed/36376157.
16. Hu P, Gao Y, Zhang Y, Sun K. Ultrasound image-based deep learning to differentiate tubal-ovarian abscess from ovarian endometriosis cyst. Front Physiol. 2023;14:1101810. https://www.ncbi.nlm.nih.gov/pubmed/36824470.
17. Lu H, Arshad M, Thornton A, Avesani G, Cunnea P, Curry E, Kanavati F, Liang J, Nixon K, Williams ST, et al. A mathematical-descriptor of tumor-mesoscopic-structure from computed-tomography images annotates prognostic- and molecular-phenotypes of epithelial ovarian cancer. Nat Commun. 2019;10(1):764. https://www.ncbi.nlm.nih.gov/pubmed/30770825.
18. Sun R, Limkin EJ, Vakalopoulou M, Dercle L, Champiat S, Han SR, Verlingue L, Brandao D, Lancia A, Ammari S, et al. A radiomics approach to assess tumour-infiltrating CD8 cells and response to anti-PD-1 or anti-PD-L1 immunotherapy: an imaging biomarker, retrospective multicohort study. Lancet Oncol. 2018;19(9):1180–91. https://www.ncbi.nlm.nih.gov/pubmed/30120041.
19. Dohan A, Gallix B, Guiu B, Le Malicot K, Reinhold C, Soyer P, Bennouna J, Ghiringhelli F, Barbier E, Boige V, et al. Early evaluation using a radiomic signature of unresectable hepatic metastases to predict outcome in patients with colorectal cancer treated with FOLFIRI and bevacizumab. Gut. 2020;69(3):531–9. https://www.ncbi.nlm.nih.gov/pubmed/31101691.
20. Thomas AA, Arevalo-Perez J, Kaley T, Lyo J, Peck KK, Shi W, Zhang Z, Young RJ. Dynamic contrast enhanced T1 MRI perfusion differentiates pseudoprogression from recurrent glioblastoma. J Neurooncol. 2015;125(1):183–90. https://www.ncbi.nlm.nih.gov/pubmed/26275367.
21. Zhang M, Gulotta B, Thomas A, Kaley T, Karimi S, Gavrilovic I, Woo KM, Zhang Z, Arevalo-Perez J, Holodny AI, et al. Large-volume low apparent diffusion coefficient lesions predict poor survival in bevacizumab-treated glioblastoma patients. Neuro Oncol. 2016;18(5):735–43. https://www.ncbi.nlm.nih.gov/pubmed/26538618.
22. Liu J, Wang Y, Liu Y, Liu Z, Cui Q, Ji N, Sun S, Wang B, Wang Y, Sun X, et al. Immunohistochemical profile and prognostic significance in primary central nervous system lymphoma: analysis of 89 cases. Oncol Lett. 2017;14(5):5505–12. https://www.ncbi.nlm.nih.gov/pubmed/29113178.
23. Qi Z, Duan L, Yuan G, Liu J, Li J, Li G, Yu Y, Xu Y, Ma S, Pan Y, et al. Clinical impact of the histopathological index and neuroimaging features status in primary central nervous system diffuse large B-Cell lymphoma: a single-center retrospective analysis of 51 cases. Front Oncol. 2022;12:769895. https://www.ncbi.nlm.nih.gov/pubmed/35875161.
24. Jin X, Zheng X, Chen D, Jin J, Zhu G, Deng X, Han C, Gong C, Zhou Y, Liu C, et al. Prediction of response after chemoradiation for esophageal cancer using a combination of dosimetry and CT radiomics. Eur Radiol. 2019;29(11):6080–8. https://www.ncbi.nlm.nih.gov/pubmed/31028447.
25. Vickers AJ, Van Calster B, Steyerberg EW. Net benefit approaches to the evaluation of prediction models, molecular markers, and diagnostic tests. BMJ. 2016;352:i6. https://www.ncbi.nlm.nih.gov/pubmed/26810254.
26. Schaff LR, Grommes C. Primary central nervous system lymphoma. Blood. 2022;140(9):971–9. https://www.ncbi.nlm.nih.gov/pubmed/34699590.
27. Cheng G, Zhang J. Imaging features (CT, MRI, MRS, and PET/CT) of primary central nervous system lymphoma in immunocompetent patients. Neurol Sci. 2019;40(3):535–42. https://www.ncbi.nlm.nih.gov/pubmed/30580380.
28. Zhao H, Ma M, Zhang L, Zheng G, Lv H, Liu J, Li X, Song B, Zhang G. Diagnosis of central nervous system lymphoma via cerebrospinal fluid cytology: a case report. BMC Neurol. 2019;19(1):90. https://www.ncbi.nlm.nih.gov/pubmed/31064334.
29. Hatzoglou V, Oh JH, Buck O, Lin X, Lee M, Shukla-Dave A, Young RJ, Peck KK, Vachha B, Holodny AI, et al. Pretreatment dynamic contrast-enhanced MRI biomarkers correlate with progression-free survival in primary central nervous system lymphoma. J Neurooncol. 2018;140(2):351–8. https://www.ncbi.nlm.nih.gov/pubmed/30073640.
30. Grommes C, DeAngelis LM. Primary CNS Lymphoma. J Clin Oncol. 2017;35(21):2410–8. https://www.ncbi.nlm.nih.gov/pubmed/28640701.
31. Holdhoff M, Mrugala MM, Grommes C, Kaley TJ, Swinnen LJ, Perez-Heydrich C, Nayak L. Challenges in the treatment of newly diagnosed and recurrent primary Central Nervous System Lymphoma. J Natl Compr Canc Netw. 2020;18(11):1571–8. https://www.ncbi.nlm.nih.gov/pubmed/33152700.
32. Yang H, Xun Y, Yang A, Liu F, You H. Advances and challenges in the treatment of primary central nervous system lymphoma. J Cell Physiol. 2020;235(12):9143–65. https://www.ncbi.nlm.nih.gov/pubmed/32420657.
33. Luchini C, Pantanowitz L, Adsay V, Asa SL, Antonini P, Girolami I, Veronese N, Nottegar A, Cingarlini S, Landoni L, et al. Ki-67 assessment of pancreatic neuroendocrine neoplasms: systematic review and meta-analysis of manual vs. digital pathology scoring. Mod Pathol. 2022;35(6):712–20. https://www.ncbi.nlm.nih.gov/pubmed/35249100.
34. Raverot G, Ilie MD, Lasolle H, Amodru V, Trouillas J, Castinetti F, Brue T. Aggressive pituitary tumours and pituitary carcinomas. Nat Rev Endocrinol. 2021;17(11):671–84. https://www.ncbi.nlm.nih.gov/pubmed/34493834.
35. Lenschow C, Schrägle S, Kircher S, Lorenz K, Machens A, Dralle H, Riss P, Scheuba C, Pfestroff A, Spitzweg C, et al. Clinical presentation, treatment, and outcome of parathyroid carcinoma. Ann Surg. 2022;275(2):e479–87.
36. Lee ES, Jung SY, Kim JY, Kim JJ, Yoo TK, Kim YG, Lee KS, Lee ES, Kim EK, Min JW, et al. Identifying the potential long-term survivors among breast cancer patients with distant metastasis. Ann Oncol. 2016;27(5):828–33.
37. Mukai H, Yamaguchi T, Takahashi M, Hozumi Y, Fujisawa T, Ohsumi S, Akabane H, Nishimura R, Takashima T, Park Y, et al. Ki-67 response-guided preoperative chemotherapy for HER2-positive breast cancer: results of a randomised phase 2 study. Br J Cancer. 2020;122(12):1747–53. https://www.ncbi.nlm.nih.gov/pubmed/32238920.
38. Lin X, Lee M, Buck O, Woo KM, Zhang Z, Hatzoglou V, Omuro A, Arevalo-Perez J, Thomas AA, Huse J, et al. Diagnostic accuracy of T1-Weighted dynamic contrast-Enhanced-MRI and DWI-ADC for differentiation of Glioblastoma and Primary CNS Lymphoma. AJNR Am J Neuroradiol. 2017;38(3):485–91. https://www.ncbi.nlm.nih.gov/pubmed/27932505.
39. Harreld JH, Hwang SN, Qaddoumi I, Tatevossian RG, Li X, Dalton J, Haupfear K, Li Y, Ellison DW. Relative ADC and location differ between posterior Fossa Pilocytic Astrocytomas with and without gangliocytic differentiation. AJNR Am J Neuroradiol. 2016;37(12):2370–5. https://www.ncbi.nlm.nih.gov/pubmed/27469209.
40. Chen H, Li W, Wan C, Zhang J. Correlation of dynamic contrast-enhanced MRI and diffusion-weighted MR imaging with prognostic factors and subtypes of breast cancers. Front Oncol. 2022;12:942943. https://www.ncbi.nlm.nih.gov/pubmed/35992872.

41. Hu XX, Yang ZX, Liang HY, Ding Y, Grimm R, Fu CX, Liu H, Yan X, Ji Y, Zeng MS, et al. Whole-tumor MRI histogram analyses of hepatocellular carcinoma: correlations with Ki-67 labeling index. J Magn Reson Imaging. 2017;46(2):383–92. https://www.ncbi.nlm.nih.gov/pubmed/27862582.
42. Schob S, Meyer J, Gawlitza M, Frydrychowicz C, Muller W, Preuss M, Bure L, Quaschling U, Hoffmann KT, Surov A. Diffusion-weighted MRI reflects proliferative activity in primary CNS lymphoma. PLoS ONE. 2016;11(8):e0161386. https://www.ncbi.nlm.nih.gov/pubmed/27571268.
43. Schmitz F, Voigtlander H, Strauss D, Schlemmer HP, Kauczor HU, Jang H, Sedaghat S. Differentiating low- and high-proliferative soft tissue sarcomas using conventional imaging features and radiomics on MRI. BMC Cancer. 2024;24(1):1589. https://www.ncbi.nlm.nih.gov/pubmed/39736582.
44. Chen M, Cao J, Hu J, Topatana W, Li S, Juengpanich S, Lin J, Tong C, Shen J, Zhang B, et al. Clinical-radiomic analysis for pretreatment prediction of Objective Response to First Transarterial Chemoembolization in Hepatocellular Carcinoma. Liver Cancer. 2021;10(1):38–51. https://www.ncbi.nlm.nih.gov/pubmed/33708638.
45. Bera K, Braman N, Gupta A, Velcheti V, Madabhushi A. Predicting cancer outcomes with radiomics and artificial intelligence in radiology. Nat Rev Clin Oncol. 2022;19(2):132–46. https://www.ncbi.nlm.nih.gov/pubmed/34663898.
46. Li G, Li L, Li Y, Qian Z, Wu F, He Y, Jiang H, Li R, Wang D, Zhai Y, et al. An MRI radiomics approach to predict survival and tumour-infiltrating macrophages in gliomas. Brain. 2022;145(3):1151–61. https://www.ncbi.nlm.nih.gov/pubmed/35136934.
47. Wang Y, Liu F, Wu S, Sun K, Gu H, Wang X. CTA-Based Radiomics and Area Change Rate Predict Infrarenal Abdominal aortic aneurysms patients events: a Multicenter Study. Acad Radiol. 2024;31(8):3165–76. https://www.ncbi.nlm.nih.gov/pubmed/38307789.
48. Sun K, Wang Y, Shi R, Wu S, Wang X. An ensemble machine learning model assists in the diagnosis of gastric ectopic pancreas and gastric stromal tumors. Insights Imaging. 2024;15(1):225. https://www.ncbi.nlm.nih.gov/pubmed/39320559.
49. Gomes Candido Reis D, Levy D, Lage L, Culler HF, Rocha V, Bydlowski SP, Nogueira Zerbini MC, Pereira J. New genetic prognostic biomarkers in primary central nervous system lymphoma (PCNSL). Brain Behav. 2021;11(4):e02061. https://www.ncbi.nlm.nih.gov/pubmed/33591648.
50. Zhao E, Yang YF, Bai M, Zhang H, Yang YY, Song X, Lou S, Yu Y, Yang C. MRI radiomics-based interpretable model and nomogram for preoperative prediction of Ki-67 expression status in primary central nervous system lymphoma. Front Med (Lausanne) 2024, 111345162https://www.ncbi.nlm.nih.gov/pubmed/38994341
51. Lambin P, Leijenaar RTH, Deist TM, Peerlings J, de Jong EEC, van Timmeren J, Sanduleanu S, Larue R, Even AJG, Jochems A, et al. Radiomics: the bridge between medical imaging and personalized medicine. Nat Rev Clin Oncol. 2017;14(12):749–62. https://www.ncbi.nlm.nih.gov/pubmed/28975929.
52. Gore S, Chougule T, Jagtap J, Saini J, Ingalhalikar M. A review of Radiomics and Deep Predictive modeling in Glioma characterization. Acad Radiol. 2021;28(11):1599–621. https://www.ncbi.nlm.nih.gov/pubmed/32660755.
53. Xia W, Hu B, Li H, Geng C, Wu Q, Yang L, Yin B, Gao X, Li Y, Geng D. Multiparametric-MRI-Based Radiomics Model for differentiating primary Central Nervous System Lymphoma from Glioblastoma: Development and Cross-vendor Validation. J Magn Reson Imaging. 2021;53(1):242–50. https://www.ncbi.nlm.nih.gov/pubmed/32864825.
54. Bathla G, Priya S, Liu Y, Ward C, Le NH, Soni N, Maheshwarappa RP, Monga V, Zhang H, Sonka M. Radiomics-based differentiation between glioblastoma and primary central nervous system lymphoma: a comparison of diagnostic performance across different MRI sequences and machine learning techniques. Eur Radiol. 2021;31(11):8703–13. https://www.ncbi.nlm.nih.gov/pubmed/33890149.
55. Kang D, Park JE, Kim YH, Kim JH, Oh JY, Kim J, Kim Y, Kim ST, Kim HS. Diffusion radiomics as a diagnostic model for atypical manifestation of primary central nervous system lymphoma: development and multicenter external validation. Neuro Oncol. 2018;20(9):1251–61. https://www.ncbi.nlm.nih.gov/pubmed/29438500.
56. Dong D, Fang MJ, Tang L, Shan XH, Gao JB, Giganti F, Wang RP, Chen X, Wang XX, Palumbo D, et al. Deep learning radiomic nomogram can predict the number of lymph node metastasis in locally advanced gastric cancer: an international multicenter study. Ann Oncol. 2020;31(7):912–20. https://www.ncbi.nlm.nih.gov/pubmed/32304748.

Publisher's note